Preprint Title $CuO/ZnFe_2O_4$ heterostructure as efficient catalyst for $NaBH_4$ - assisted reduction of Chloramphenicol

Authors Hoa T. Le, Huong T. T. Nguyen, Viet Q. Le, Dat N. Trinh, Cuong D. Nguyen, Nhi T. T. Le and Hoa T. Tran

Publication Date 26 Juni 2026

Article Type Full Research Paper

ORCID® iDs Hoa T. Le - https://orcid.org/0000-0002-1359-187X; Nhi T. T. Le - https://orcid.org/0009-0007-5078-6151; Hoa T. Tran - https://orcid.org/0000-0003-4814-4364

CuO/$ZnFe_2O_4$ heterostructure as efficient catalyst for $NaBH_4$ - assisted reduction of Chloramphenicol

*Hoa T. Le[1], Huong TT Nguyen[1], Viet Q. Le[1], Dat N. Trinh[2], Cuong D. Nguyen[3], Nhi TT Le [*4,5] and Hoa T. Tran[*1]*

[1]*University of Sciences, Hue University, Hue City 530000, Vietnam*

[2]*The University of Danang, University of Science and Education, Danang city, 550000, Vietnam*

[3]*University of Education, Hue University, Hue City 530000, Viet Nam*

[4]*Center for Advanced Chemistry, Institute of Research and Development, Duy Tan University, 03 Quang Trung, Danang city, 550000, Vietnam*

[5]*Faculty of Natural Sciences, Duy Tan University, 03 Quang Trung, Danang city, 550000,Vietnam*

Correspondence: *tthaihoa@hueuni.edu.vn ; letthanhnhi1@duytan.edu.vn*

Abstract

In this study, CuO/$ZnFe_2O_4$ heterostructure in the form of flower, consisting of CuO nanorods anchored on $ZnFe_2O_4$ microspheres, was successfully synthesized and evaluated for its catalytic reduction of chloramphenicol (CAP) in the presence of $NaBH_4$. Structural and morphological analysis confirmed the successful formation of the heterostructure with enhanced contact between $ZnFe_2O_4$ and CuO. Compared to pure $ZnFe_2O_4$, the CuO/$ZnFe_2O_4$ catalyst exhibited significantly improved catalytic activity for CAP reduction. The reduction efficiency was strongly influenced by reaction conditions, with optimal performance achieved at pH 6, a catalyst dosage of 2.5 g/L, and a short reaction time of 20 minutes. The enhanced catalytic performance under mild, environmentally friendly conditions highlights the crucial role of CuO in promoting surface electron transfer and facilitating reduction. Kinetic analysis at room temperature revealed a shift from pseudo-first-order to zero-order kinetics throughout the reaction, suggesting surface-mediated catalysis. This evolution indicates that decatalysis is primarily governed by a surface-mediated Langmuir–Hinshelwood mechanism. Overall, the CuO/$ZnFe_2O_4$ heterostructure shows significant potential as an efficient catalyst for rapid CAP reduction under neutral conditions, offering a promising strategy for wastewater treatment.

Graphical abstract

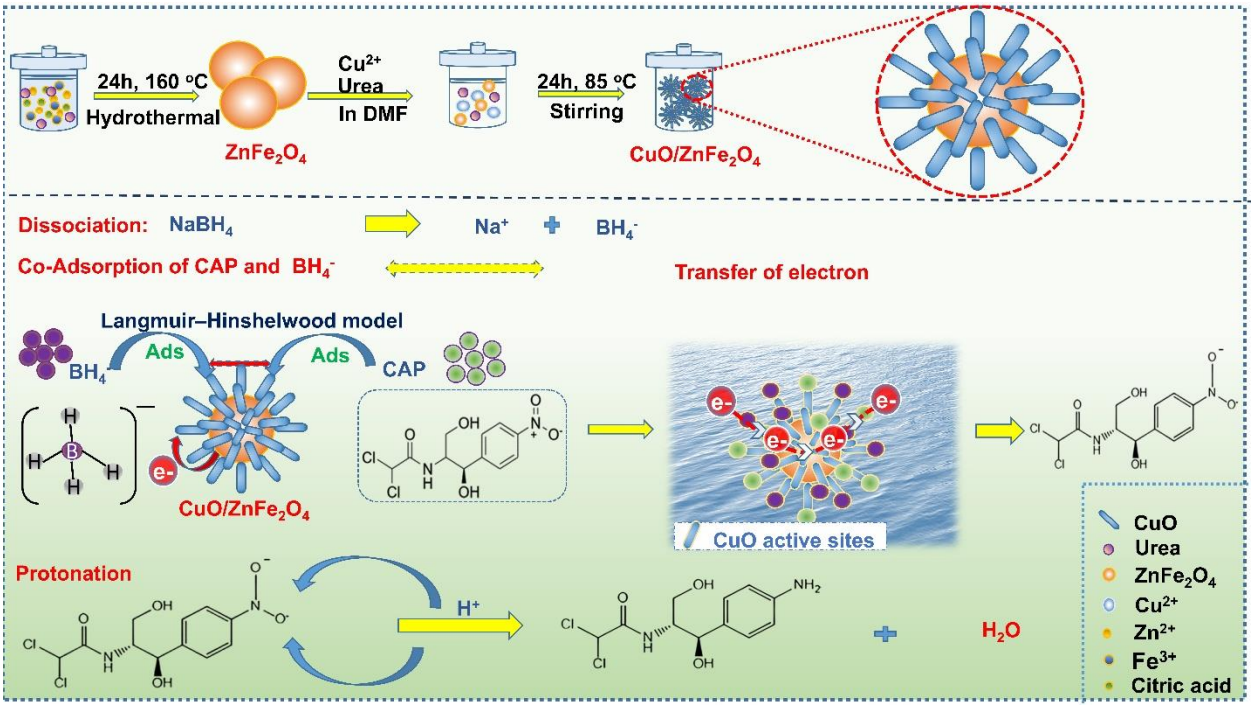

Key words: $ZnFe_2O_4$, CuO, Chloramphenicol, catalytic, reduction, $NaBH_4$

1. Introduction

The rapid expansion of agro-industrial sectors, including textile, chemical, fertilizer, pesticide, and pharmaceutical industries, has led to the continuous discharge of large amounts of organic pollutants (OPs) into aquatic environments. Among these, antibiotic residues are of particular concern due to their persistence and resistance to conventional biological treatment processes. These compounds are often only partially removed, remaining either in treated effluents or temporarily retained in activated sludge, from which they can subsequently be released back into the environment [1]. Chloramphenicol (CAP), a broad-spectrum antibiotic effective against both Gram-positive and Gram-negative bacteria, has been widely used in medical and veterinary applications. However, its presence in water systems poses serious health risks, as CAP has been associated with severe toxic effects in humans, including bone marrow suppression and, in extreme cases, fatal aplastic anemia [2]. Therefore, the effective removal of these contaminants from water bodies is critical.

Various treatment technologies have been developed to address organic pollutants, including membrane separation, biodegradation, adsorption, and catalytic processes. Among these methods, catalytic reduction has attracted considerable attention due to its operational simplicity, cost-effectiveness, high efficiency, and ease of scaling from laboratory studies to practical applications. In recent years, organic pollutants containing nitro groups have received much attention in this field, as the -NO_2 functional group can be selectively reduced to less toxic amino derivatives. In this context, sodium borohydride ($NaBH_4$) has been widely used as a strong hydrogen donor for reduction conversions [3]. However, in the absence of a catalyst, the reduction process is kinetically unfavorable. Therefore, catalytic surfaces, especially those based on metal nanostructures or metal oxides, play a crucial role in facilitating electron transfer and enabling the efficient delivery of active hydrogen species from BH_4^- to pollutant molecules [4].

Magnetic nanoparticles (MNP) are one of the magnetic metal nanoparticles widely used in catalysis for environmental treatment. MNPs can be synthesized through different compositions and phases, including pure metals such as Fe, Co, and Ni; metal oxides such as Fe_3O_4, γ Fe_2O_3; ferrites such as MFe_2O_4 (M = Cu, Ni, Mn, Mg, etc.); and metal alloys of ferrites such as FePt and CoPt [5]. Among them, $ZnFe_2O_4$ (a form of MNP) is considered a magnetic semiconductor that can act catalytically in the visible light region because it has a narrow band gap energy (E_g = 1.92 eV) with an electric potential (valence band (VB) at 0.38 V, and conduction band (CB) at −1.54 V) [6]. The structure of nano-sized $ZnFe_2O_4$ has a spinel structure, with Zn^{2+} positions tending to occupy tetrahedral positions, and Fe^{3+} ions will occupy octahedral positions in the crystal lattice. The mutual distribution between cations at these two positions significantly impacts the electronic, magnetic, and catalytic properties of $ZnFe_2O_4$. Besides, the Zn^{2+} ion appears to be non-toxic and has electronic inert properties that provide high photochemical stability to $ZnFe_2O_4$. In general, $ZnFe_2O_4$ has many outstanding characteristics, such as magnetism, optical properties, non-toxicity, and stability in many different environments [7]. However, at the nanoscale, $ZnFe_2O_4$ is often unstable due to its tendency to aggregate and undergo surface oxidation, which can reduce its dispersibility and magnetic performance over time. To overcome these limitations, various surface

functionalization and structural modification strategies have been developed to improve stability and dispersibility, thereby enhancing catalytic efficiency. Based on these considerations, the development of efficient and stable catalysts based on $ZnFe_2O_4$ spinel ferrite coupled with transition-metal oxides is a potential approach to overcome existing limitations. Among them, CuO is a p-type semiconductor with a narrow energy gap (1.2-2.1 eV), high stability, good conductivity, low cost, and relatively low toxicity [8], and has proven effective in applications such as energy storage, antimicrobial and photocatalysis [9]. Therefore, the combination of $ZnFe_2O_4$ and CuO is expected to improve catalytic activity by enhancing surface reactivity and promoting electron transfer. In this study, the $CuO/ZnFe_2O_4$ heterostructure was designed and synthesized to enhance the catalytic reduction efficiency of CAP in the presence of $NaBH_4$. The influence of key reaction parameters, including pH, catalyst dosage, and reaction time, was systematically investigated to evaluate the efficiency of treating nitro-containing organic compounds.

Experimental section

Material

Chloramphenicol (CAP, $C_{11}H_{12}Cl_2N_2O_5$), $ZnCl_2$, $FeCl_3.6H_2O$, N,N′-dimethylformamide (DMF), $CuCl_2.2H_2O$, urea (CON_2H_4), NaCl and citric acid ($C_6H_8O_7$) were purchased from Merck (Germany). No additional purification was performed on the analytical reagents before use, and all experimental procedures used deionized water.

Synthesis of $ZnFe_2O_4$ NPs

$ZnFe_2O_4$ is synthesized by the hydrothermal method. After being mixed well, the mixture of ethylene glycol (60 mL), $ZnCl_2$ (0.28 g), $FeCl_3.6H_2O$ (1.08 g), urea (2 g) and citric acid (0.5 g) will be transferred to an autoclave lined with 100 mL stainless steel Teflon and heated for 24 hours at 160 °C. After cooling to room temperature, the resulting solid was filtered, washed with deionized water, and dried in an oven for 6 h at 60 °C. The resulting solid was transferred to a muffle furnace at 400 ^{o}C for 2 h, and the sample was further washed and dried for 6 h at 60 ^{o}C [10].

Synthesis of $CuO/ZnFe_2O_4$

$ZnFe_2O_4$ (600 mg) was added to a solution containing $CuCl_2.2H_2O$ (540 mg) and Urea (1.0 g) dissolved in DMF (60 mL). The mixture was homogenized using an ultrasonic device for 10 minutes. Then, this homogeneous solution was transferred to a heat-resistant vessel in an autoclave and heated at 85°C for 24 h. The product collected by centrifugation (10,000 rpm, 5 mins) will be washed with DMF and acetone several times. Finally, $CuO/ZnFe_2O_4$ was dried overnight at room temperature.

Characterization

The crystal structure of the composite materials was analyzed by X-ray diffraction (XRD; Bruker AXS, Germany) using Cu Kα radiation (λ = 1.5406 Å) over the 2θ range of 10 - 80°. Before analysis, the powder samples were lightly ground and spread evenly on a sample holder to ensure a flat and uniform surface. The surface morphology and microstructure of the samples were examined by scanning electron microscopy (SEM, Hitachi S-4800, Japan). The surface chemical composition and elemental state were studied using X-ray photoelectron spectroscopy (XPS; K-Alpha, Thermo VG, United Kingdom) with monochromated Al Kα radiation as the excitation source.

Catalytic experiments

In the catalytic decomposition experiment, 40 mL of CAP solution (30 mg/L) at a set pH was mixed with a specified amount of catalyst. Next, 5 mL of $NaBH_4$ solution (60 mM) was added, and distilled water was added to reach a total volume of 100 mL. The mixture was stirred at 150 rpm. After every 2 minutes, the solids were magnetically separated, and 2.5 mL of supernatant was collected for CAP concentration measurement. The removal efficiency was evaluated using the ratio C_t/C_0, decreasing from 1 to 0 as efficiency increased. The effects of time (5-50 min), pH (4-10), catalyst dosage (0-4 g/L), and ion strength with NaCl concentration (0.1-0.4 M), on removal efficiency were systematically studied to find optimal conditions.

2. Results and discussion

2.1. Characterization

The crystal structure and phase composition of $ZnFe_2O_4$ and $CuO/ZnFe_2O_4$ were studied by X-ray diffraction (XRD). As shown in Figure 1, the diffraction peaks of pure $ZnFe_2O_4$ located at $2\theta = 29.9°$, 35.2°, 42.9°, 53.8°, 57.0° and 62.2° can be identified as the (220), (311), (400), (422), (511) and (440) planes of cubic $ZnFe_2O_4$ spinel (PDF#22-1012), indicating the successful formation of well-crystallized $ZnFe_2O_4$ [11] [12]. For the $CuO/ZnFe_2O_4$ composite material, all characteristic diffraction peaks of $ZnFe_2O_4$ appear, meaning the spinel structure of $ZnFe_2O_4$ remains intact after the formation of the composite material. Several new diffraction peaks appear at 2θ = 36.1°, 38.9°, 52.9°, 61.7°, and 66.2°, assigned to the planes (002), (111), (020), (113), and (311) of monoclinic CuO (PDF#48-1548), respectively [13] [14]. The coexistence of $ZnFe_2O_4$ and CuO diffraction features confirms the successful construction of the $CuO/ZnFe_2O_4$ heterostructure, in which CuO is effectively incorporated without disrupting the $ZnFe_2O_4$ crystal framework.

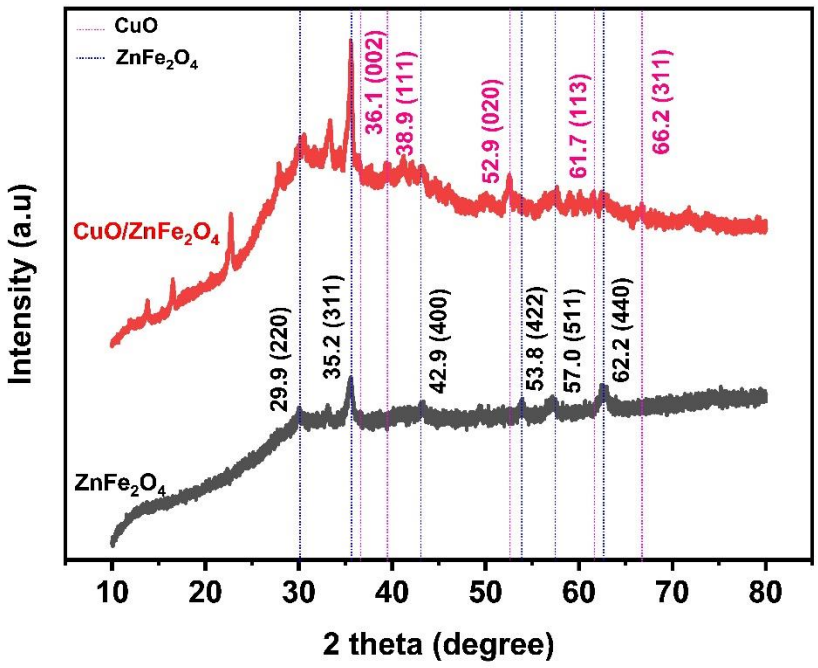

Figure 1: XRD patterns of $ZnFe_2O_4$ and $CuO/ZnFe_2O_4$.

While XRD analysis confirmed the phase composition and crystal structure of the $ZnFe_2O_4$ and $CuO/ZnFe_2O_4$ samples, XPS analysis clarified the surface elemental composition, chemical states, and electronic interactions at the interface between $ZnFe_2O_4$ and CuO.

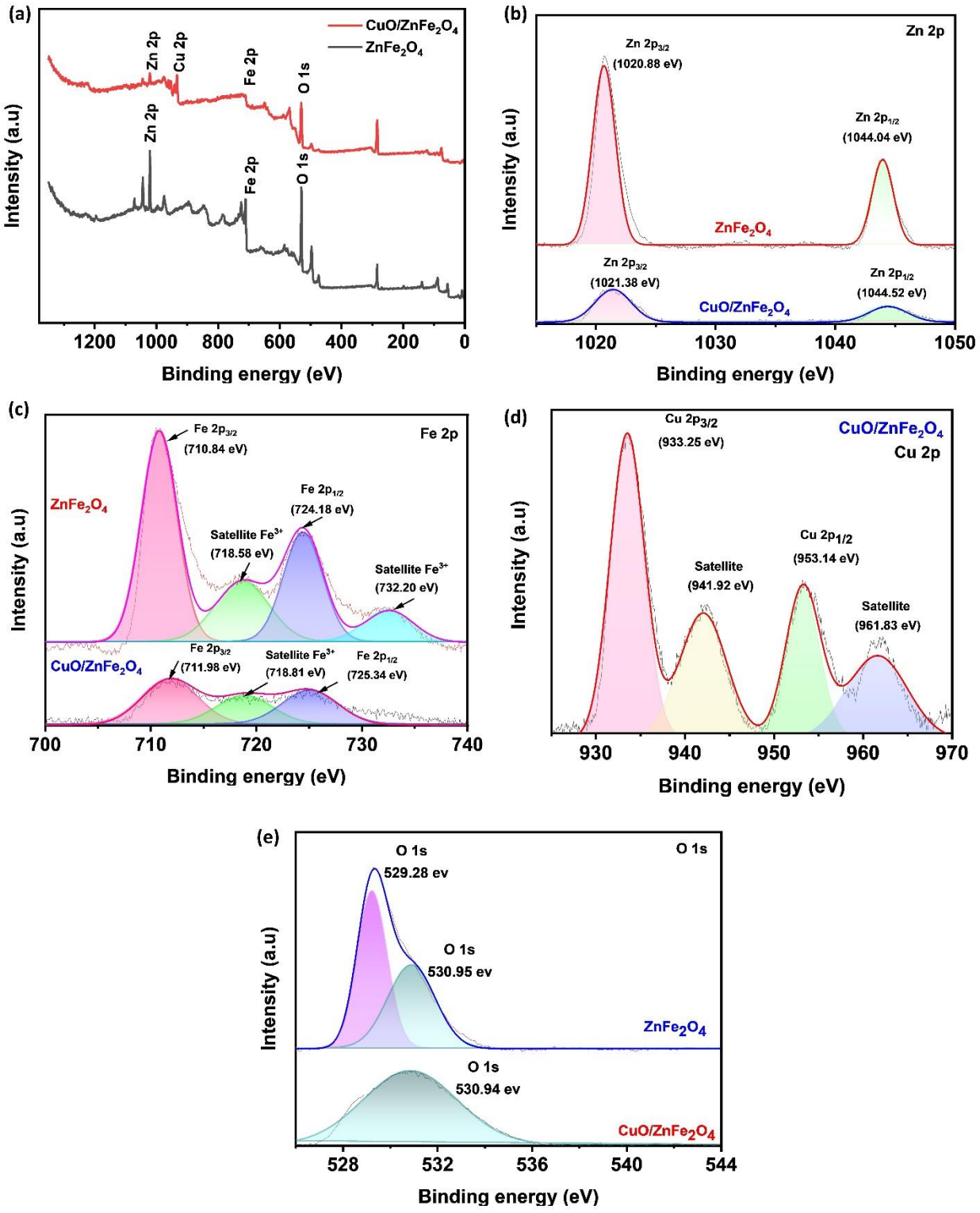

Figure 2: XPS spectra of: (a) survey; (b) Zn2p and (c) Fe2p for $ZnFe_2O_4$ and $CuO/ZnFe_2O_4$; (d) Cu2p for $CuO/ZnFe_2O_4$ and (e) O1s for $ZnFe_2O_4$ and $CuO/ZnFe_2O_4$.

The generalized XPS spectra of $ZnFe_2O_4$ and $CuO/ZnFe_2O_4$ (**Figure 2a**) show the presence of the elements Zn, Fe, and O in the pure $ZnFe_2O_4$ sample, while the additional appearance of Cu signals in the $CuO/ZnFe_2O_4$ spectrum confirms the successful incorporation of CuO into the $ZnFe_2O_4$ matrix and the formation of a heterostructured composite material. The high-resolution XPS spectra of Zn 2p for both samples (**Figure 2b**) show two characteristic peaks located in the ranges of 1044.04-1044.52 eV and 1020.88-1021.38 eV, assigned to the energy levels of Zn $2p_1/_2$ and Zn $2p_3/_2$, respectively [15]. The spin-orbit energy split and the positions of these peaks are consistent with the Zn^{2+} oxidation state, indicating that the chemical state of zinc remains unchanged after the formation of the $CuO/ZnFe_2O_4$ composite [16]. The high-resolution Fe 2p spectra of pure $ZnFe_2O_4$ (**Figure 2c**) show two main peaks at 710.84 and 724.18 eV, corresponding to Fe $2p_3/_2$ and Fe $2p_1/_2$, respectively. Furthermore, the appearance of two satellite peaks at approximately 718.58 and 732.20 eV is characteristic of Fe^{3+} ions, arising from a shake-up excitation $^+$ in the spinel structure. This confirms the dominant presence of Fe^{3+} in $ZnFe_2O_4$, consistent with previous reports on ferrite synthesized by hydrothermal methods, in which the oxidation of Fe^{2+} and the formation of heterogeneous Fe-O coordination environments can occur [17]. In contrast, the Fe 2p spectrum of the $CuO/ZnFe_2O_4$ composite material, besides the two main peaks of Fe $2p_3/_2$ and Fe $2p_1/_2$, only a single Fe^{3+} satellite peak is observed at approximately 718.81 eV. The attenuation or disappearance of the satellite peak in the higher binding energy region may suggest to strong interfacial interactions between $ZnFe_2O_4$ and CuO, leading to a redistribution of electron density and the stabilization of Fe^{3+} species at the heterojunction. Additionally, spectral overlap and partial surface coverage of $ZnFe_2O_4$ by CuO can attenuate the Fe $2p_1/_2$ satellite peak intensity. Similar suppression of Fe^{3+} satellite peaks have been observed in many ferrite-based composite systems and is often associated with charge transport effects at the interface [16] [18]. The high-resolution XPS spectrum of Cu 2p in the $CuO/ZnFe_2O_4$ composite material (**Figure 2d**) shows peaks at 933.25 eV and 953.14 eV, with spin-orbit energy splitting of 19.89 eV, respectively assigned to Cu $2p_3/_2$ and Cu $2p_1/_2$, characteristic of Cu^{2+} ions. In addition, the presence of distinct shake-up satellite peaks at 941.92 eV and 961.83 eV provides compelling evidence for the

formation of CuO and unambiguously excludes the existence of Cu_2O phases, in good agreement with previous reports [19]. The O 1s spectrum of pure $ZnFe_2O_4$ is resolved into two components at ~529.28 and 530.94 eV (**Figure 2e**). The lower binding energy (529.28 eV) corresponds to lattice oxygen (O^{2-}) in Zn-O and Fe-O bonds within the spinel structure, while the higher binding energy peak is related to surface oxygen species, oxygen defects, or adsorbed hydroxyl groups [15]. By comparison, the O 1s spectrum of $CuO/ZnFe_2O_4$ is dominated by a single dominant peak at ~530.94 eV, attributed to the overlap of oxygen species from $ZnFe_2O_4$ and CuO lattices as well as interface oxygen defects. The emergence of this unified O 1s feature indicates strong interfacial interaction and effective electronic coupling between $ZnFe_2O_4$ and CuO, consistent with the Cu^{2+}-dominated chemical environment revealed by the pronounced Cu 2p shake-up satellite structure [20]. While XPS provided strong evidence for the chemical states and confirmed the successful formation of the $CuO/ZnFe_2O_4$ composite, SEM was employed to further elucidate the surface morphology and assess the spatial distribution of the CuO phase on the $ZnFe_2O_4$ matrix. As illustrated in Figure 3, the $CuO/ZnFe_2O_4$ material exhibits flower-like hierarchical microstructures with an average size of approximately 4 μm. These structures are formed by the assembly of densely packed CuO nanorods radiating outward from the surface, resulting in a rough and highly textured morphology. Compared with $ZnFe_2O_4$ (inset), which displays a relatively compact, granular surface, the incorporation of CuO significantly alters the surface architecture, increasing surface roughness. Such hierarchical heterostructures are expected to provide more accessible active sites and facilitate interfacial electron transfer [21] during catalytic reaction.

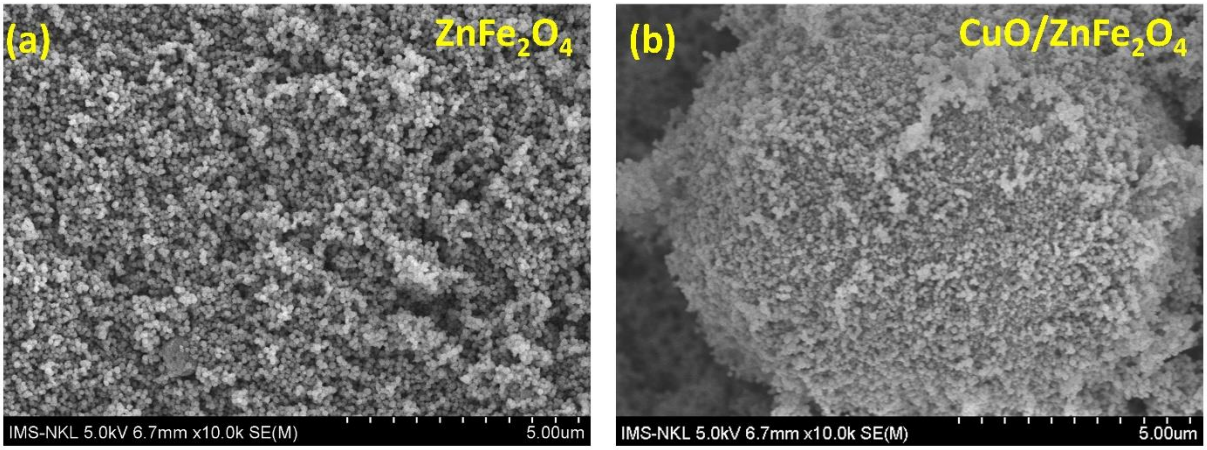

Figure 3: The SEM images of $ZnFe_2O_4$ (a) and $CuO/ZnFe_2O_4$ (b). The scale bar is 5 μm for both images.

Catalytic activity

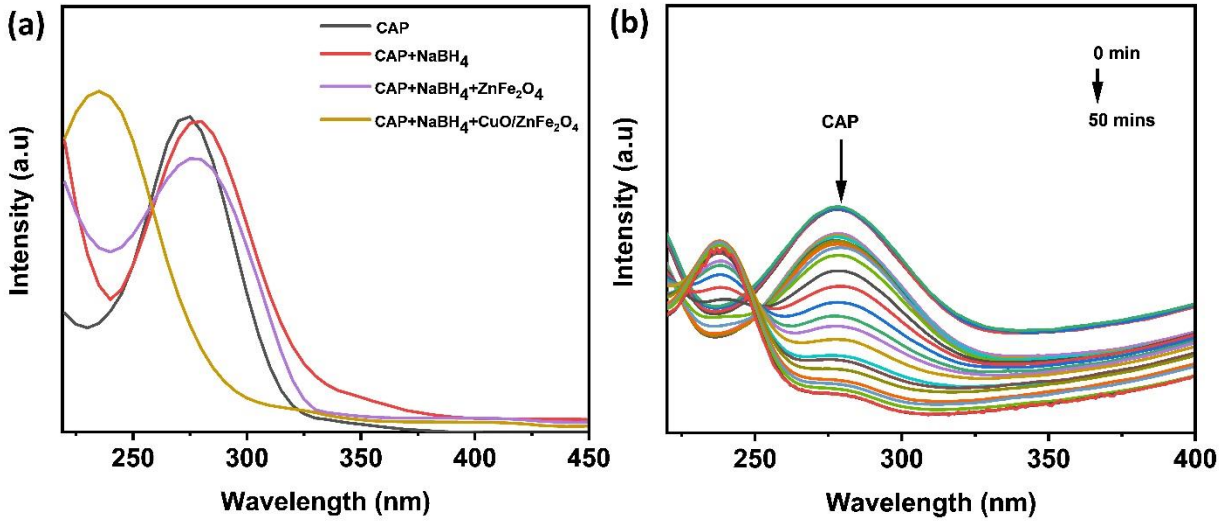

Figure 4: UV-Vis spectra of the CAP solution before and after the removal processes (a) of $ZnFe_2O_4$ and $CuO/ZnFe_2O_4$; (b) of $CuO/ZnFe_2O_4$ in 50 min reaction.

The catalytic reduction of CAP was investigated using $NaBH_4$ as the electron donor and $ZnFe_2O_4$ and $CuO/ZnFe_2O_4$ as heterogeneous catalysts. The reaction progression was monitored through the UV-Vis spectral changes of CAP under different conditions (CAP, CAP + $NaBH_4$, CAP + $NaBH_4$ + $ZnFe_2O_4$, and CAP + $NaBH_4$ + $CuO/ZnFe_2O_4$) in **Figure 4a**, allowing for a systematic comparison of the influence of each component on the reaction

process. The results show that $NaBH_4$ did not cause a significant change in the absorption spectrum of CAP, reflecting the kinetic limitations of the direct reduction process. In the presence of $ZnFe_2O_4$, the absorption intensity at 280 nm only slightly decreases without the appearance of a new absorption band, indicating limited interaction and catalytic activity. Conversely, in the $CuO/ZnFe_2O_4$ catalytic system, the characteristic absorption peak of CAP at approximately 280 nm disappears completely, and a strong new absorption band appears at ~236 nm, indicating a significant change in the optical properties of the CAP molecule. This phenomenon is consistent with previous reports on the reduction of nitro compounds by $NaBH_4$, where the presence of a solid catalyst plays a key role in regulating electron transfer and overcoming the kinetic barrier of the reaction [22] [23]. The kinetic change of the reduction process is more clearly shown in **Figure 4b**, which depicts the decrease in the absorption intensity of CAP at 280 nm over reaction time after the addition of $CuO/ZnFe_2O_4$ in the presence of $NaBH_4$. The absorption intensity decreases continuously throughout reaction period, indicating that CAP is efficiently converted under these catalytic conditions. These results confirm that the $CuO/ZnFe_2O_4$ system exhibits superior catalytic activity compared to $ZnFe_2O_4$ alone, and highlight the role of CuO in enhancing the CAP reduction efficiency in the $NaBH_4$ system.

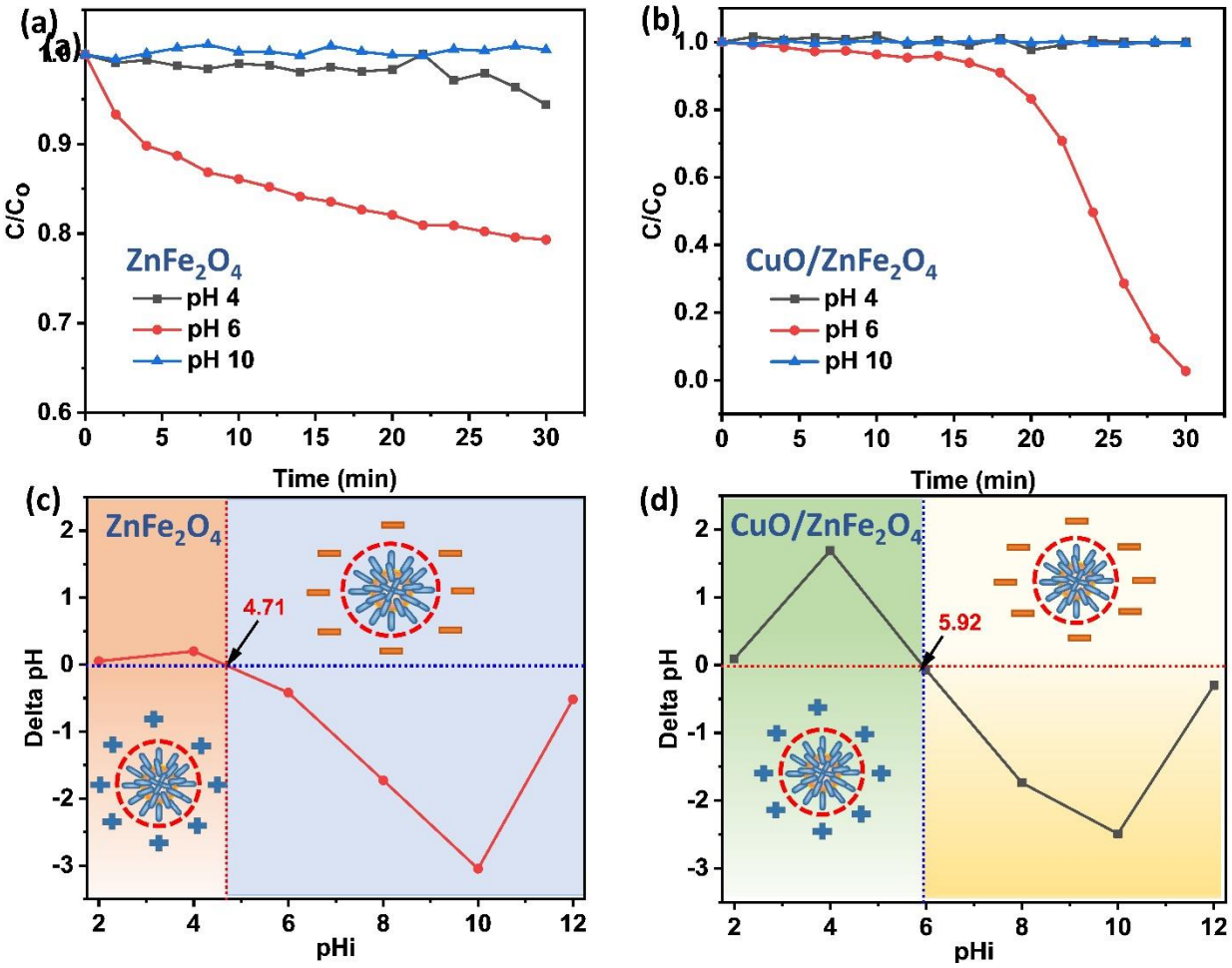

Figure 5: Effect of pH (a,b) for the reduction of CAP; pH_{PZC} of $ZnFe_2O_4$ (c) and $CuO/ZnFe_2O_4$ (d).

The results of the pH effect survey (**Figure 5**) show that catalytic reduction activity is strongly dependent on the reaction environment and the material's surface nature. For $ZnFe_2O_4$, the absorption spectrum did not change significantly over time within the investigated pH range (pH 4, 6, and 10), indicating that this material does not exhibit significant catalytic activity but mainly acts as an adsorbent. This suggests that $ZnFe_2O_4$ does not provide sufficient active sites for electron transfer from BH_4^- to the CAP molecule, consistent with previous reports on unmodified spinel oxides, which typically exhibit limited catalytic activity and primarily act as adsorbents or supports unless modified or combined with active components [24]. Conversely, the $CuO/ZnFe_2O_4$ system exhibits a significant pH dependence, with the highest observed at pH = 6. Specifically,

under this condition, the ratio C/C_o decreases significantly, indicating not only rapid CAP removal but also the formation of intermediates characteristic of the multi-step surface-medicated transformation mechanism on the catalyst surface. This difference can be explained by the ionization state of CAP and the material's surface charge properties. At neutral pH, with a pK_a of 5.5 [25], CAP mainly exists in the molecular or semionized form, which is favorable for surface interactions. At the same time, the incorporation of CuO shifts the isoelectric point (pH_{pzc}) from 4.71 to 5.92, indicating that the composite surface becomes less negative under the same pH conditions. The enhanced activity at pH 6 may be due to a balanced surface charge, which reduces repulsion towards BH_4^- while maintaining effective CAP adsorption, thereby facilitating surface interaction and electron transfer. Conversely, unfavorable charge conditions at pH 4 and 10 may limit adsorption or reactivity, thereby reducing catalytic performance. These observations suggest that pH not only affects the ionization state of CAP but also the catalyst's surface charge, thereby impacting catalytic efficiency. Furthermore, the incorporation of CuO may create redox active sites that facilitate electron transfer [26], which may explain the enhanced catalytic performance of $CuO/ZnFe_2O_4$ compared to $ZnFe_2O_4$.

Figure 6 illustrates the effect of catalyst dosage (2.0, 2.5, and 3.0 g/L) on the catalytic removal efficiency of CAP in the presence of $NaBH_4$. Compared with the dosage of 2.0 g/L, increasing the $CuO/ZnFe_2O_4$ loading to 2.5 and 3.0 g/L significantly enhanced both the removal efficiency and the reaction rate throughout the catalytic process. Specifically, the system containing 2.0 g/L of catalyst required approximately 30 min to achieve high CAP removal efficiency, whereas the reaction time was shortened to 20 min and 22 min for catalyst dosages of 2.5 and 3.0 g/L, respectively. The improved catalytic performance at higher catalyst loadings can be attributed to the increased availability of CuO active sites and enlarged surface area, which facilitate the transfer of BH_4^- species and reactive electrons toward CAP molecules, thereby accelerating the reduction process [26]. However, when the catalyst dosage exceeded 2.5 g/L, the catalytic activity enhancement became insignificant and even declined slightly. This behavior is likely associated with the limited amount of $NaBH_4$ in the reaction system, which restricts the generation of

active hydrogen species and the transfer of electrons required for the reduction reaction [27]. Therefore, a catalyst dosage of 2.5 g/L was selected as the optimal condition for subsequent experiments.

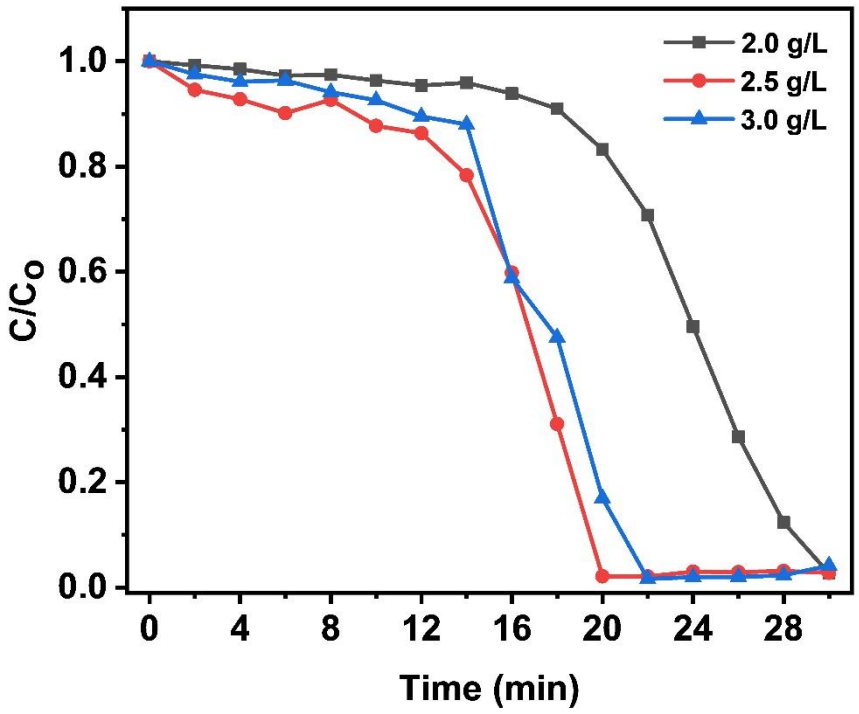

Figure 6: The effect of catalytic dose for catalytic reduction of $CuO/ZnFe_2O_4$ at different dose of 2 g/L, 2.5 g/L and 3 g/L.

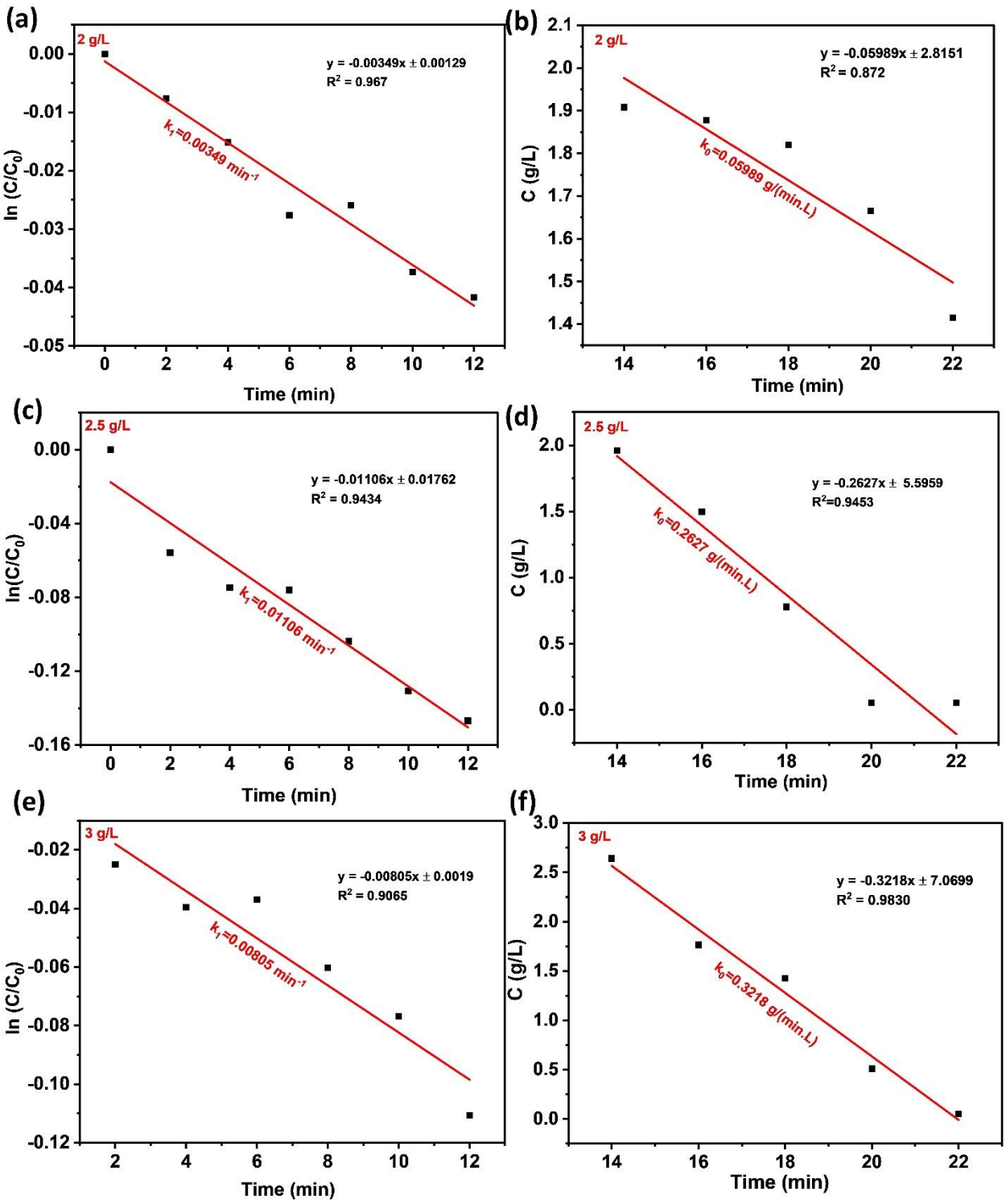

Figure 7: The kinetic for catalytic reduction of $CuO/ZnFe_2O_4$ at different dose of 2 g/L (a,b), 2.5 g/L (c,d) and 3 g/L (e,f) at room temperature.

Kinetic analysis results (**Figure 7a–f**) at three catalyst dosages of 2, 2.5, and 3 g/L at room temperature showed that the CAP catalytic reduction reaction on the $CuO/ZnFe_2O_4$ system did not follow a single kinetic regime throughout the reaction. In the initial phase (0 - 12 minutes), the reaction exhibited good linearity with a pseudo-first-order kinetic model (**Figure 7a, c, and e** corresponding to 2, 2.5, and 3 g/L, respectively), with a correlation coefficient (R^2) higher than 0.9. This phenomenon may be due to the excess concentration of $NaBH_4$ in the solution, while the concentration of BH_4^- remained almost constant in the initial phase of the reaction. Under these conditions, the reduction rate depended primarily on the CAP concentration and the number of surface-active sites. In later reaction stages, the reaction kinetics tend to deviate gradually from pseudo-first-order kinetics and are better described by zero-order kinetics (**Figure 7b, d, and f**), with high correlation coefficients ($R^2 > 0.9$). This shift suggests that the catalytic process is gradually dominated by surface-related phenomena rather than solely by reactant concentrations. The initial reduction follows pseudo-first-order kinetics due to excess $NaBH_4$ concentration. In later stages, deviations from first-order kinetics and a tendency toward zero-order kinetics are observed, possibly due to saturation of catalytically active sites and surface coverage by reactant intermediates or borate species. This behavior is consistent with the Langmuir–Hinshelwood (L-H) surface reaction model. According to the L-H mechanism, both BH_4^- ions and CAP molecules undergo adsorption–desorption equilibrium on the catalyst surface before the desurfacing step. In the initial stage, the catalyst surface remains relatively unsaturated, resulting in clear pseudo-first-order behavior. As the reaction progresses, increasing surface coverage by adsorbents and borate by-products can partially clog the active sites, thus limiting further acceleration of the reaction and leading to the appearance of zero-order kinetic properties. Similar kinetic transitions have been reported in $NaBH_4$-assisted decatalytic systems involving metal nanocatalysts and metal oxides [28] [29]. Among the systems studied, a catalyst dosing of 2.5 g/L showed the highest catalytic activity, achieving the highest CAP removal efficiency within 20 minutes. This result indicates that the chosen dosage provides an optimal

balance between accessible active sites and reactive hydrogen species generated from $NaBH_4$.

Different concentrations of NaCl were added to the CAP solution to evaluate the effect of ionic strength on the catalytic activity of $CuO/ZnFe_2O_4$. As shown in Figure 8, both the decomposition efficiency and the rate of CAP reduction were strongly affected by ionic strength. As the NaCl concentration increased from 0.1 to 0.4 M, the reduction process became slower, requiring a longer reaction time to achieve equivalent removal efficiency. At relatively low ionic strengths, the electrolyte had only a minor effect on the catalytic reduction of CAP; However, a pronounced inhibitory effect was observed at higher ionic strengths, especially at 0.4 M. This phenomenon suggests that excess ions in solution may hinder the interaction between BH_4^-, CAP and the $CuO/ZnFe_2O_4$ surface, thus inhibiting adsorption and electron transfer through the surface during catalysis, affecting catalytic efficiency [30]. Overall, these results indicate that the $CuO/ZnFe_2O_4$ heterostructure exhibits more favorable catalytic performance under low ionic strength conditions.

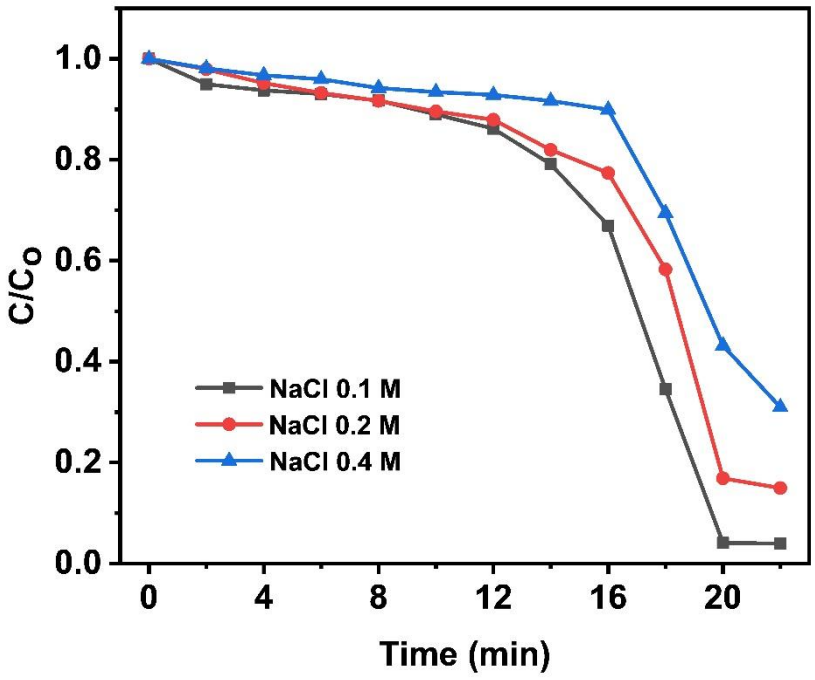

Figure 8: The effect of ion strength for the removal of CAP.

According to **Table 1**, the $CuO/ZnFe_2O_4$ system achieves a significantly shorter reaction time of only 20 minutes, demonstrating rapid reduction under neutral conditions. Photocatalytic systems like $Ce(MoO_4)_2$/GO and Ag/TiO_2 require longer reaction times and depend on external light irradiation. MOF-based and nZVI/GO systems, though efficient, often need higher catalyst dosages or extended processing times. $CuO/ZnFe_2O_4$ stands out due to its fast kinetics, neutral pH operation, and independence from light, making it promising for practical $NaBH_4$ reduction.

Table 1. Comparison of the reduction for CAP by different materials

Material	Condition	Catalytic	Light source	Reference
$Ce(MoO_4)_2$/GO	pH= 5; C_{CAP} = 20 mg/L; t = 50 min	photocatalytic	visible	[31]
Ag/TiO_2	pH= 6.5; C_{CAP} =20 mg/L; t= 120 min	photocatalytic	UV-C	[2]
PS	pH= 3; C_{CAP} = 0.03mM; t = 120 min	UV/PS oxidation	UV	[32]
Al-MIL	pH= 5.4; C_{CAP} = 80 mg/L; t = 120 min	PS oxidation	-	[33]
nZVI/GO	pH= 5; C_{CAP} = 100 mg/L; t = 180 min	photocatalytic	-	[34]
$CuO/ZnFe_2O_4$	pH= 6; C_{CAP} = 30 mg/L; t = 20 min	$NaBH_4$-Reduction	-	This study

3.2. Mechanism

Previous studies have demonstrated that aromatic nitro compounds can be reduced to their corresponding amino derivatives using $NaBH_4$ [35] [36]. Based on these findings, Scheme 1 illustrates the proposed CAP reduction pathway on the $CuO/ZnFe_2O_4$ heterostructure. Initially, $NaBH_4$ dissociates to form BH_4^- species, which interact with the catalyst surface and provide active hydrogen and electrons for the reduction reaction. Simultaneously, CAP molecules are adsorbed onto the

$CuO/ZnFe_2O_4$ surface, allowing electron transfer between interfaces and subsequent hydrogenation reactions. As illustrated in Scheme 1, the nitro group ($-NO_2$) of the CAP undergoes stepwise electron/proton transfer, ultimately forming the corresponding amino derivative ($-NH_2$) and H_2O.

Kinetic analysis revealed that the initial reduction followed pseudo-first-order kinetics due to excess $NaBH_4$ concentration, while a gradual transition to zero-order kinetics was observed in later stages. This kinetic evolution suggests a gradual occupation of catalytically active sites by adsorbed intermediates or borate species generated in the reaction. This behavior is consistent with the L-H surface reaction mechanism, in which both BH_4^- species and CAP molecules participate in an adsorption–desorption equilibrium before the surface-mediated reduction step. Overall, the $CuO/ZnFe_2O_4$ heterostructure provides favorable interface active sites for adsorption, electron transfer, and catalytic hydrogenation in the $NaBH_4$ system. The proposed mechanism is also consistent with previously reported catalytic reduction pathways for nitro-containing organic compounds [37].

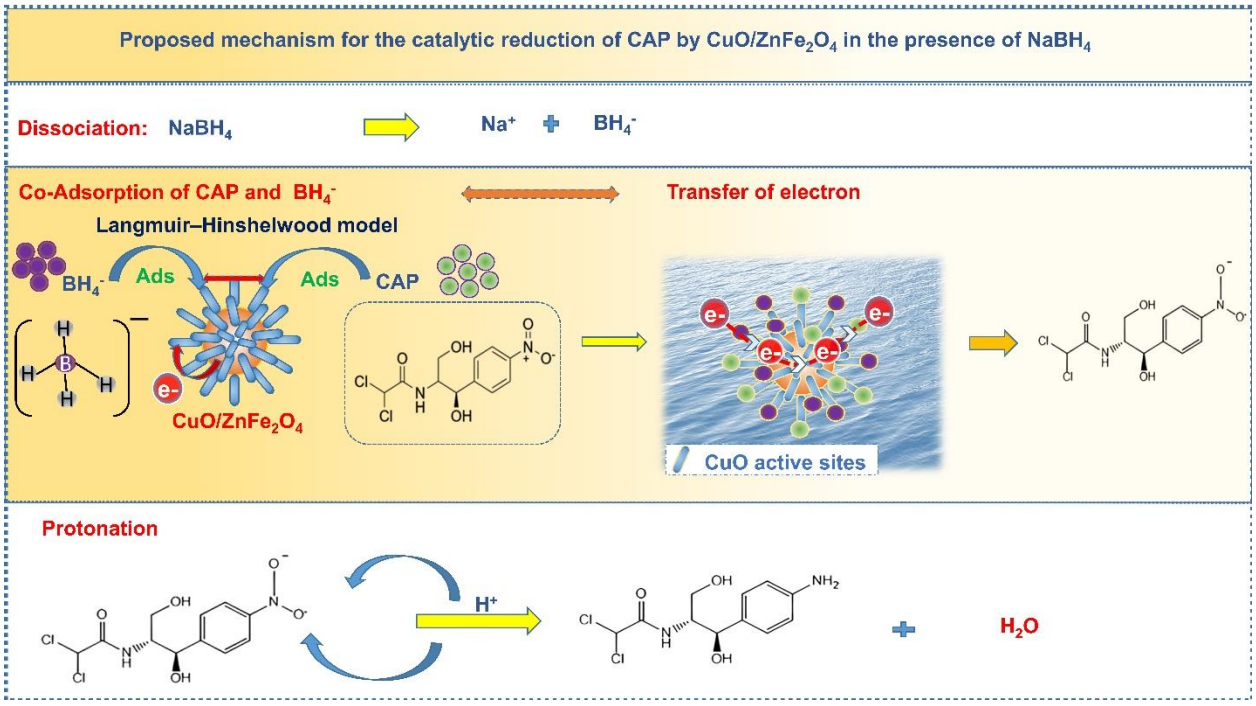

Scheme 1: The proposed mechanism of catalytic reduction for CAP reduction**.**

Conclusion

The $CuO/ZnFe_2O_4$ heterostructure was synthesized with a flower-like morphology composed of CuO nanorods uniformly distributed over the $ZnFe_2O_4$ surface. In the presence of $NaBH_4$, the $CuO/ZnFe_2O_4$ system displayed markedly enhanced catalytic reduction efficiency for CAP compared to pristine $ZnFe_2O_4$, reaching maximum performance at pH 6, a catalyst loading of 2.5 g/L, and a reaction period of 20 min. This increased catalytic activity results from the integration of CuO, which supplies highly active sites and accelerates interfacial electron transfer during reduction. Kinetic analysis revealed a transition from pseudo-first-order behavior at the initial stage to zero-order kinetics at later stages, suggesting the involvement of surface-mediated catalytic processes associated with adsorption equilibrium and progressive surface coverage during the reaction. This behavior is consistent with the Langmuir-Hinshelwood surface reaction model. Overall, these findings demonstrate that the $CuO/ZnFe_2O_4$ heterostructure provides favorable interfacial properties for efficient CAP catalytic reduction in the $NaBH_4$ system, offering rapid treatment efficiency and promising potential for practical wastewater remediation applications.

Funding

This research is funded by Vietnam National Foundation for Science and Technology Development (NAFOSTED) under grant number 104.06-2021.60.

Declaration of competing interest

The authors declare no potential conflicts of interest.

ORCID iDs

Hoa Tran Thai https://orcid.org/0000-0003-4814-4364

Author Contributions

All authors contributed to the research idea and design. Material preparation, data collection, and analysis were performed by L.T.H, N.T.T.H, L.Q.V, T.N.D, N.D.C, L.T.T.N., and T.T.H. The first draft was written by L.T.H, L.T.T.N, and T.T.H. All authors reviewed and approved the final draft.

Data Availability Statement: The data that supports the findings of this study is available from the corresponding author upon reasonable request.

References

(1) Elmolla, E. S.; Chaudhuri, M. *Desalination* **2010**, *252*, 46–52. doi:10.1016/j.desal.2009.11.003

(2) Jodat, A.; Jodat, A. *Desalin. Water Treat.* **2014**, *52*, 2668–2677. doi:10.1080/19443994.2013.794115

(3) Ravikumar, K. V. G.; Dubey, S.; pulimi, M.; Chandrasekaran, N.; Mukherjee, A. *J. Mol. Liq.* **2016**, *224*, 589–598. doi:10.1016/j.molliq.2016.10.040

(4) Ecevit, H.; Altun, T. *J. Water Process Eng.* **2025**, *76*, 108177. doi:10.1016/j.jwpe.2025.108177

(5) Aghayi-Anaraki, M.; Safarifard, V. *Fe3O4@MOF Magnetic Nanocomposites: Synthesis and Applications*; 2020; Vol. 2020. doi:10.1002/ejic.202000012

(6) Tao, R.; Zhao, C.; Shao, C.; Li, X.; Li, X.; Zhang, J.; Yang, S.; Liu, Y. *Mater. Res. Bull.* **2018**, *104*, 124–133. doi:10.1016/j.materresbull.2018.03.041

(7) Liu, Z.; Fan, T.; Zhou, H.; Zhang, D.; Gong, X.; Guo, Q.; Ogawa, H. *Bioinspir. Biomim.* **2007**, *2*, 30–35. doi:10.1088/1748-3182/2/1/004

(8) Li, L.; Chen, X.; Quan, X.; Qiu, F.; Zhang, X. *ACS Omega* **2023**, *8*, 2723–2732. doi:10.1021/ACSOMEGA.2C07364

(9) Singh, J.; Soni, R. K. *Appl. Surf. Sci.* **2020**, *521*, 146420. doi:10.1016/j.apsusc.2020.146420

(10) Niaki, Z. M.; Ghorbani, M.; Ghoreishi, S. A. *J. Environ. Heal. Sci. Eng.* **2021**, *19*, 1583–1596. doi:10.1007/s40201-021-00713-x

(11) Wang, K.; Chen, Q.; Xie, H.; Wang, M.; Kong, X.; Cheng, K.; Jin, Z. *Catal. Letters* **2024**, *154*, 6227–6240. doi:10.1007/s10562-024-04830-8

(12) Huerta-Aguilar, C. A.; Diaz-Puerto, Z. J.; Tecuapa-Flores, E. D.; Thangarasu, P. *ACS Omega* **2022**, *7*, 33985–34001. doi:10.1021/acsomega.2c03153

(13) Wang, X.; Han, Q.; Cai, S.; Wang, T.; Qi, C.; Yang, R.; Wang, C. *Analyst* **2017**, *142*, 2500–2506. doi:10.1039/c7an00589j

(14) Zhu, D.; Wang, L.; Yu, W.; Xie, H. *Sci. Rep.* **2018**, *8*, 1–12. doi:10.1038/s41598-018-23174-z

(15) Nikolic, M. V.; Vasiljevic, Z. Z.; Lukovic, M. D.; Pavlovic, V. P.; Krstic, J. B.; Vujancevic, J.; Tadic, N.; Vlahovic, B.; Pavlovic, V. B. *Int. J. Appl. Ceram. Technol.* **2019**, *16*, 981–993. doi:10.1111/ijac.13190

(16) Xu, Y.; Wu, S.; Li, X.; Huang, Y.; Wang, Z.; Han, Y.; Wu, J.; Meng, H.; Zhang, X. *New J. Chem.* **2017**, *41*, 15433–15438. doi:10.1039/c7nj03373g

(17) Chen, H.; Liu, W.; Qin, Z. *Catal. Sci. Technol.* **2017**, *7*, 2236–2244. doi:10.1039/c7cy00308k

(18) Zhou, X.; Li, X.; Sun, H.; Sun, P.; Liang, X.; Liu, F.; Hu, X.; Lu, G. *ACS Appl. Mater. Interfaces* **2015**, *7*, 15414–15421. doi:10.1021/acsami.5b03537

(19) Boruban, C.; Esenturk, E. N. *J. Nanoparticle Res.* **2018**, *20*. doi:10.1007/s11051-018-4139-0

(20) Padil, V. V. T.; Černík, M. *Int. J. Nanomedicine* **2013**, *8*, 889–898. doi:10.2147/IJN.S40599

(21) Solanki, K.; Sharma, S.; Yadav, S.; Kaushik, B.; Rana, P.; Dixit, R.; Sharma, R. K. *Small* **2023**, *19*, 2300394. doi.org/10.1002/smll.202300394

(22) Guo, W.; Zheng, Y.; Xiang, W.; Zhang, Y. *RSC Sustain.* **2024**, *3*, 243–254. doi:10.1039/d4su00531g

(23) Nachaichot, A.; Kenvised, O.; Choram, S.; Nijpanich, S.; Budsombat, S. *RSC Adv.* **2025**, *15*,

6974–6983. doi:10.1039/d5ra00081e

(24) Zhang, K.; Suh, J. M.; Choi, J. W.; Jang, H. W.; Shokouhimehr, M.; Varma, R. S. *ACS Omega* **2019**, *4*, 483–495. doi:10.1021/acsomega.8b03051

(25) Mohd Din, A. T.; Ahmad, M. A.; Hameed, B. H. *Chem. Eng. J.* **2015**, *260*, 730–739. doi:10.1016/j.cej.2014.09.010

(26) Li, Y.; Wang, Y.; Lu, H.; Li, X. *Int. J. Hydrogen Energy* **2020**, *45*, 16080–16093. doi:10.1016/j.ijhydene.2020.04.002

(27) Mirshafiee, F.; Rezaei, M. *Sci. Rep.* **2024**, *14*, 1–15. doi:10.1038/s41598-024-60428-5

(28) Wunder, S.; Polzer, F.; Lu, Y.; Mei, Y.; Ballauff, M. *J. Phys. Chem. C* **2010**, *114*, 8814–8820. doi:10.1021/jp101125j

(29) Andrieux, J.; Demirci, U. B.; Miele, P. *Catal. Today* **2011**, *170*, 13–19. doi:10.1016/j.cattod.2011.01.019

(30) Kottappara, R.; Pillai, S. C.; Kizhakkekilikoodayil Vijayan, B. *Inorg. Chem. Commun.* **2020**, *121*, 108181. doi:10.1016/j.inoche.2020.108181

(31) Karthik, R.; Vinoth Kumar, J.; Chen, S. M.; Karuppiah, C.; Cheng, Y. H.; Muthuraj, V. *ACS Appl. Mater. Interfaces* **2017**, *9*, 6547–6559. doi:10.1021/acsami.6b14242

(32) Tan, C.; Fu, D.; Gao, N.; Qin, Q.; Xu, Y.; Xiang, H. *J. Photochem. Photobiol. A Chem.* **2017**, *332*, 406–412. doi:10.1016/j.jphotochem.2016.09.021

(33) Geçgel, C.; Görmez, Ö.; Gözmen, B.; Turabik, M.; Kalderis, D. *Chemosphere* **2022**, *308*. doi:10.1016/j.chemosphere.2022.136411

(34) Idham, M. F.; Falyouna, O.; Eljamal, R.; Maamoun, I.; Eljamal, O. *J. Water Process Eng.* **2022**, *50*, 103289. doi:10.1016/j.jwpe.2022.103289

(35) Colón, D.; Weber, E. J.; Anderson, J. L.; Winget, P.; Suárez, L. A. *Environ. Sci. Technol.* **2006**, *40*, 4449–4454. doi:10.1021/es0600429

(36) Zeynizadeh, B.; Mohammadzadeh, I.; Shokri, Z.; Ali Hosseini, S. *J. Colloid Interface Sci.* **2017**, *500*, 285–293. doi:10.1016/j.jcis.2017.03.030

(37) Edebali, S. *Appl. Surf. Sci. Adv.* **2023**, *18*, 100496. doi:10.1016/j.apsadv.2023.100496